nature energy

Perspective

https://doi.org/10.1038/s41560-025-01745-5

Scaling and heating will drive low-temperature CO_2 electrolysers to operate at higher temperatures

Received: 30 October 2024

Accepted: 24 February 2025

Published online: 28 April 2025

Check for updates

Henri M. Pelzer, Nikita Kolobov, David A. Vermaas & Thomas Burdyny

Low-temperature carbon dioxide electrolysis (CO_2E) provides a one-step means of converting CO_2 into carbon-based fuels using electrical inputs at temperatures below 100 °C. Over the past decade, an abundance of work has been carried out at ambient temperature, and high CO_2E rates and product selectivities have been achieved. With scaling of CO_2E technologies underway, greater discourse surrounding heat management and the viable operating temperatures of larger systems is important. In this Perspective we argue that, owing to the energy inefficiency of electrolysers, heat generation in CO_2E stacks will favour operating temperatures of between 40 and 70 °C, far from the ambient temperatures used so far. Such elevated temperatures put further pressure on catalyst and membrane stability and on the stack design. On the other hand, elevated temperatures could alleviate challenges in salt precipitation, water management and high cell voltages, aiding the technology. We reflect on these aspects and discuss the opportunities for waste heat valorization to increase the economic feasibility of the process.

The heavy decarbonization of society is essential for maintaining and improving the standard of living of humankind. One key sector for decarbonization is the chemical industry, which relies heavily on fossil fuel resources such as oil and natural gas[1]. Many chemicals are carbon-based, making carbon neutrality particularly challenging. One potential low-carbon pathway for producing base chemicals is carbon dioxide electrolysis (CO_2E), utilizing green energy and captured CO_2. CO_2E is capable of selectively producing chemical building blocks such as carbon monoxide (CO) and ethylene[2].

Low-temperature CO_2E is currently well-established on the laboratory scale, with larger cell and stack demonstrations becoming more frequent[3]. The most efficient and scalable configurations utilize a CO_2 gas-fed membrane electrode assembly (MEA) 'zero gap' cell. Whereas bipolar membranes hold promise for providing a stable KOH anolyte, enabling the use of earth-abundant anode materials, anion exchange membranes (AEMs) are still commonly applied[4]. At elevated current densities, reported state-of-the-art energy efficiencies range from 30 to 60% (refs. 5,6), leading to cell voltages of between 2.3 and 4.7 V (ref. 7). If water acts as a proton donor the energy efficiency is thermodynamically limited to a maximum of 62% (ref. 6). Thus, approximately 40–70% of the input electricity is dissipated as heat, which is substantially higher than the approximately 35% value of proton exchange membrane (PEM) water electrolysers with a similar architecture[8]. As laboratory-scale CO_2E devices are on the order of 10 W, the ~5 W of heat released goes primarily unnoticed or is reported to dissipate from the electrolyser, tubing and electrolyte. Looking to future CO_2E systems of 0.1–1 MW, however, the amount of heat to be dissipated becomes substantial and needs to be accounted for in the plant design and system integration. An additional consequence of heat generation is temperature gradients within the CO_2E stack.

Within the CO_2E research field, experiments have been conducted predominantly at ambient temperature (20–25 °C). Such accessible operating conditions have enabled researchers with different research specializations and laboratory capabilities to quickly enter the field and perform research at the 1–10 W scale. The testing of <10 W systems at higher temperatures (>40 °C) has been comparatively limited[9–11],

Department of Chemical Engineering, Delft University of Technology, Delft, Netherlands. e-mail: h.p.pelzer@tudelft.nl; t.e.burdyny@tudelft.nl

although these temperatures are near uniform in reports that use larger cells or stacks[9,12]. Recent literature reports demonstrating CO_2E stacks on the kilowatt scale[13,14], for example, have shown that the inefficiency of electrolysers causes cell and anolyte temperatures to rise rapidly to temperatures of >50 °C in the absence of active heat-removal measures, thus leading to higher operation temperatures[12]. This poses a dilemma: either operate at 20–25 °C, leveraging existing knowledge but assuming that future CO_2 electrolyser stacks will be heavily cooled, or embrace the challenges and opportunities that come with operation at elevated temperature. Such a decision impacts not only system integration and overall energetics but also the multitude of temperature-dependent parameters that influence the CO_2E performance metrics.

In this Perspective we argue that unavoidable heat generation will force even modestly sized CO_2E stacks to operate at temperatures between 40 and 70 °C. Greater research activities must then shift towards higher-temperature testing, not only to pre-emptively overcome new unexpected challenges but also to benefit from the operating regime. Although looking at electrolyser heating may appear minor at first, we show that it induces non-linear changes in CO_2 and salt solubility, vapour pressure, electrode kinetics, conductivity, water transport and catalyst stability. We close with a discussion on the potential efficiency upsides of heat recuperation on the process level.

Heat sources and sinks in CO_2 electrolysers

In state-of-the-art zero-gap MEA cells, gaseous humidified CO_2 is supplied on the cathode side. The CO_2 then diffuses through a porous layer to a liquid-immersed catalyst layer where CO_2 reduction takes place. The cathode and anode are separated by an AEM[15–17], with a liquid electrolyte positioned next to the oxygen-evolving anode. The entire thickness of the above cell components normally is <3 mm. To form a stacked electrolyser, cells are placed adjacent to one another in either a unipolar or a bipolar design (see Fig. 1a)[3]. Keeping in mind industrially relevant current density (j) values of >200 mA cm^{-2}, we can compare the sources and sinks of heat within a CO_2E stack[2,17,18].

A basic heat balance of a CO_2E stack is shown in Fig. 1a and displayed in equation (1):

$$0 = \dot{Q}_{\mathrm{gas}} + \dot{Q}_{\mathrm{liq}} + \dot{Q}_{\mathrm{surf}} - \dot{Q}_{\eta+\Omega}. \tag{1}$$

The relevant heat sources are characterized by $\dot{Q}_{\eta+\Omega}$, that is, the heat released by the excess overpotential to drive the electrochemical reactions and to overcome ohmic resistances. The entropic effects of mixing gases are ignored. The parameter $\dot{Q}_{\eta+\Omega}$ is proportional to the potential $U_{\eta+\Omega}$, which is defined as the difference between the applied cell/stack potential (U_{cell}) and the thermoneutral potential of the reaction (U_{th}). The parameter $U_{\eta+\Omega}$ is then multiplied with the total current (i) passed in the electrolyser to calculate $\dot{Q}_{\eta+\Omega}$ (equation (2)):

$$\dot{Q}_{\eta+\Omega} = U_{\eta+\Omega} i = (U_{\mathrm{cell}} - U_{\mathrm{th}})\, i. \tag{2}$$

The excess overpotential that results in heat generation occurs across the cell and can be split into several distinct components. These include reaction overpotentials of the cathode and anode reactions (η_{cath} and η_{an}, respectively), the voltage drop over the AEM (U_{AEM}), and the voltage drop over the contact resistance at the membrane–cathode interface ($U_{\mathrm{C,cath}}$) or the membrane–anode interface ($U_{\mathrm{C,an}}$) (Fig. 1b)[19,20]. Part of the required overpotentials drives the electrochemical reactions to split water, which acts as a proton donor for CO_2 reduction. Heat then dissipates when the by-product hydroxide from water splitting reacts with CO_2 to form carbonate at the cathode (see Fig. 1c). Carbonate is then itself neutralized by protons near the anode after crossing the AEM. Whereas heat is released during both of the neutralization reactions, their heating effect is effectively included within the reaction overpotentials in equation (2). On a last note, experimental data have suggested that the contact resistance values between the components are an especially important contributor to the ohmic resistance, accounting for 80% of the accumulated ohmic drop over the membrane and interfaces, stressing the importance of interface engineering[21]. Despite the relevance of η_{cath} and η_{an} for lower current densities, the kinetic part of the overpotential scales logarithmically with the applied current, decreasing its impact at higher current densities[19,20].

To achieve steady-state operation, the heat sources must be countered by heat sinks (equation (1)). In a standard CO_2E stack, the available sinks are advection via the gas stream $\dot{Q}_{\mathrm{gas}}$ on the cathode side and the liquid anolyte stream $\dot{Q}_{\mathrm{liq}}$ on the anode side. In addition, heat can leave the system via the stack's outer surface $\dot{Q}_{\mathrm{surf}}$ (Fig. 1a). All of those heat sinks require a temperature gradient to transport heat: $\dot{Q}_{\mathrm{surf}}$ is transported over the gradient between the stack temperature and ambient temperature, whereas $\dot{Q}_{\mathrm{gas}}$ and $\dot{Q}_{\mathrm{liq}}$ can be defined via the respective inlet and outlet temperatures of the gas and liquid streams. A qualitative assessment of the resistance (R_{surf}) and capacity ($C_{\mathrm{th,gas}}$ and $C_{\mathrm{th,liq}}$) values in equations (3)–(5) can then be carried out to show the contribution of each sink using an equivalent thermal resistance and thermal capacity comparison, assuming similar magnitudes of the temperature gradients[22].

$$R_{\mathrm{surf}} = \frac{1}{h_{\mathrm{eff}} A} \tag{3}$$

$$C_{\mathrm{th,gas}} = \dot{m}_{\mathrm{gas}} c_{p,\mathrm{gas}} \tag{4}$$

$$C_{\mathrm{th,liq}} = \dot{m}_{\mathrm{liq}} c_{p,\mathrm{liq}} \tag{5}$$

Whereas a detailed heat- and mass-transport analysis is beyond the scope of this work, an order-of-magnitude analysis of equations (3)–(5) indicates that the anolyte will be predominantly responsible for heat removal from an electrolyser stack (Fig. 1d). Owing to the around fourfold larger specific heat capacity (c_p) and the about 500-fold larger density (ρ) of liquid water compared with CO_2 gas, we can expect the liquid anolyte stream to remove several orders of magnitude more heat than the humidified gas stream. Similarly, surface cooling (equation (3)) can be assumed to be negligible given the poor heat transfer coefficient (h_{eff}) of, for example, natural convection and the low external surface area A of an electrolyser[22]. For stacks in particular, the external surface area increases minimally when the number of cells is increased, whereas heat generation scales in direct proportion to the total cell area. In other words, $\dot{Q}_{\mathrm{liq}} \gg (\dot{Q}_{\mathrm{gas}} + \dot{Q}_{\mathrm{surf}})$. The importance of the anolyte stream for heat removal has been demonstrated further in recent literature reports[13,14]. Understanding that the anolyte is responsible for most heat removal enables us to predict the eventual operating temperature of a larger-scale CO_2 electrolyser.

Temperature operation range and spatial distribution

The anolyte is typically recirculated over the electrolyser (Fig. 2a). Thus, while heat can be removed from the electrolyser with each pass, it will accumulate within the anolyte circuit. Without a balanced heat removal from the whole system, temperatures will quickly approach the thermal stability limits of most AEMs at 70–80 °C (refs. 21,23) and the boiling point of the anolyte at around 100 °C (see Fig. 2b). Such heat accumulation has been illustrated in a CO_2E stack that uses cooling channels between the cells to mitigate the temperature increase[14].

The two cooling choices that exist are either to cool down the CO_2E stack directly or remove heat from the anolyte circuit. Direct cooling of a large stack requires the addition of cooling channels within each unit cell. The addition of cooling channels then complicates the stack assemblies, which already require a high tolerance to prevent sealing

https://doi.org/10.1038/s41560-025-01745-5

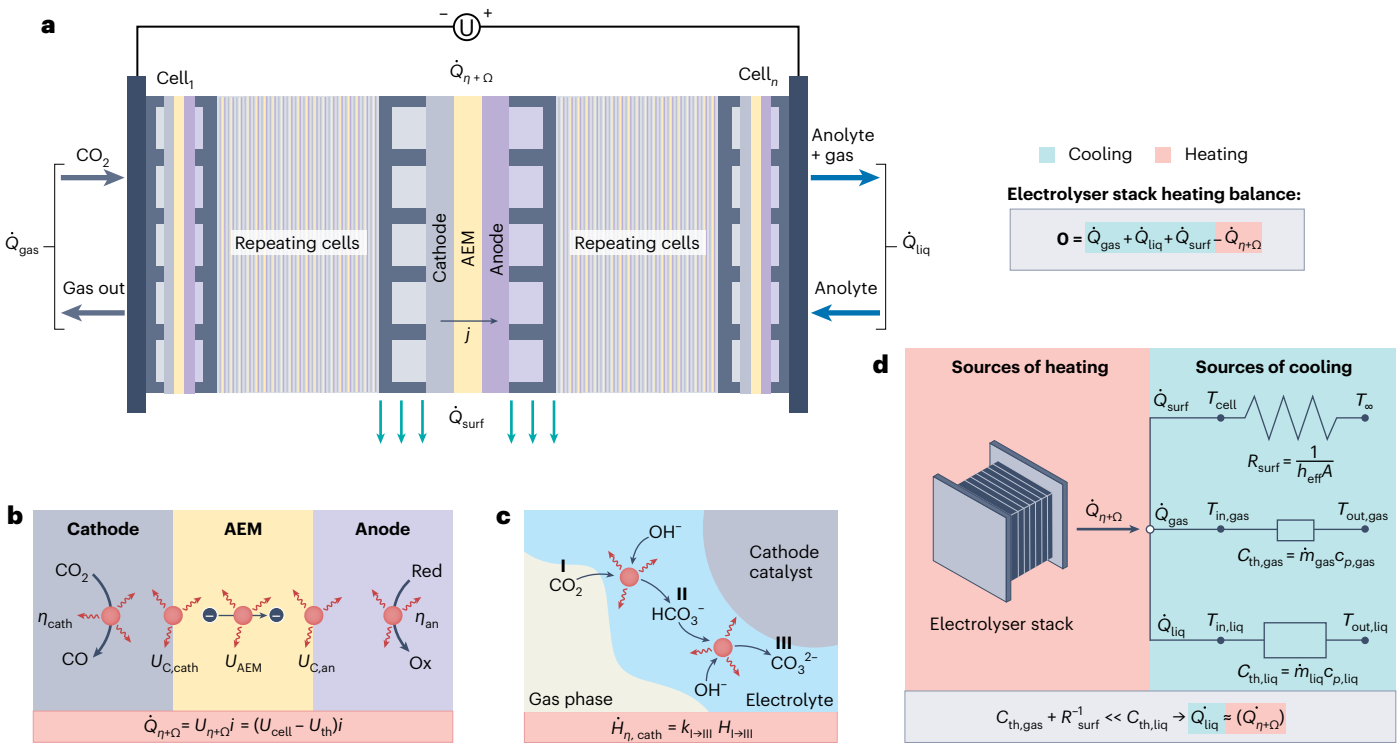

Fig. 1 | Heat balance analysis for CO_2E stack. a, Heat sinks and sources within a state-of-the-art CO_2E stack comprising of the heat transfer rates for the liquid stream $\dot{Q}_{liq}$, the gas stream $\dot{Q}_{gas}$, surface cooling $\dot{Q}_{surf}$ and cell overpotentials and ohmic losses $\dot{Q}_{\eta+\Omega}$. **b**, Location and visualization of heat generation associated with $\dot{Q}_{\eta+\Omega}$ expressed via the overpotentials and ohmic losses potential $U_{\eta+\Omega}$ and the current i. $U_{\eta+\Omega}$ can be expressed as the difference between cell voltage U_{cell} and thermoneutral potential U_{th}. Red, reduction; Ox, oxidation. **c**, As a consequence of acid–base neutralization, the resulting reaction heat transfer rate at the cathode $\dot{H}_{\eta,cath}$ is given by the reaction rate $k_{I\to III}$ and reaction enthalpy $H_{I\to III}$. **d**, Balance of heat sources and sinks showing the thermal equivalent circuit model of the respective capacities of the heat sinks via advection of the gas stream ($C_{th,gas}$) and the anolyte stream ($C_{th,liq}$), and the thermal resistance of surface cooling R_{surf}. Temperature differences are given by the streams' inlet and outlet temperatures $T_{in/out,i}$, the cell/stack temperature T_{cell} and the ambient temperature T_∞. The mass flow rates of the gas and liquid stream are given by $\dot{m}_{gas}$ and $\dot{m}_{liq}$, respectively.

and puncturing issues. However, if issue-free assembly is ensured, direct cooling poses an additional heat sink close to the heating source. Some PEM water electrolysers utilize internal stack cooling, which can act as a design basis for CO_2E stacks. The alternative method of stack cooling, namely removing heat from a liquid circuit, is well understood through traditional heat exchangers and thus poses a viable alternative[3].

Both options above require the temperature of the cooling fluid to be lower than the electrolyser temperature, which sets a lower limit for a stack's operating temperature. For heat exchangers to have a high effectiveness, the temperature difference between the anolyte circuit and the cooling fluid should be at least 10 K, with higher temperature differences more favoured economically[22]. Thus, to operate electrolysers at room temperature, chilled water (5–15 °C) would be required as a cooling source[24,25], with substantial energy costs associated with continuously cooling the source water. An alternative is to use industrial cooling water, as shown in Fig. 2b, which is more commonly available in industrial plants for a temperature range of 27–35 °C (refs. 24,25). With this range in mind, a minimum achievable steady-state $T_{anolyte}$ would be ~40 °C using a high exchange surface area. Using lower cooling rates and thus smaller heat exchanger devices or less industrial cooling water would push the steady-state $T_{anolyte}$ higher. In addition, higher operation temperatures can unlock more economic heat exchangers, for example, air/liquid heat exchangers. The upper operation limit is given by the AEM stability limit, which is typically at 70–80 °C. A membrane with increased temperature stability could extend the upper temperature limit, increasing the heat exchanger economics while providing a wider range for the optimum operation temperature. However, we argue that the operating range of CO_2 electrolysers will fall within the range of 40–70 °C.

A parallel but important discussion is the desired temperature gradient within the electrolyser itself. This aspect is illustrated in Fig. 2c where the difference between T_{in} and T_{out} is highlighted as ΔT_{SP}, the single-pass spatial temperature gradient. As the anolyte is responsible for most heat removal, the temperature difference and gradient within a stack can be adjusted via the anolyte flow rate. However, flow rates cannot be chosen freely.

The upper limit of the anolyte flow is limited by pressure drops through the system and hence the pumping cost. Simulations of different flow fields in a PEM electrolyser show that the pressure drop can increase by up to 7 bar (ref. 26). At higher pressure drops, the pressure distribution also varies more severely, leading to a spatial dependence of the differential pressure, which affects the local reaction environments[27]. In addition, the flow field needs to fulfil the role of a current collector[26]. The lower limit of the fluid flow is linked to the removal of CO_2 and O_2 gas bubbles evolving in the anolyte stream: too low a flow rate leads to gas build-up and an inhomogeneous water supply at the anode[28]. In the case where the maximum applicable flow rate does not yield sufficient cooling, the need for additional direct cooling within the stack becomes inevitable.

A separate aspect of a high ΔT_{SP} is the introduction of spatial inhomogeneities to the stack, which have multiple disadvantages. Higher spatial temperature gradients will, for example, put variable mechanical stresses on different components, shortening the lifetime of the system[29]. This local difference in ageing, together with a local dependency of current density and selectivity due to the temperature differences,

https://doi.org/10.1038/s41560-025-01745-5

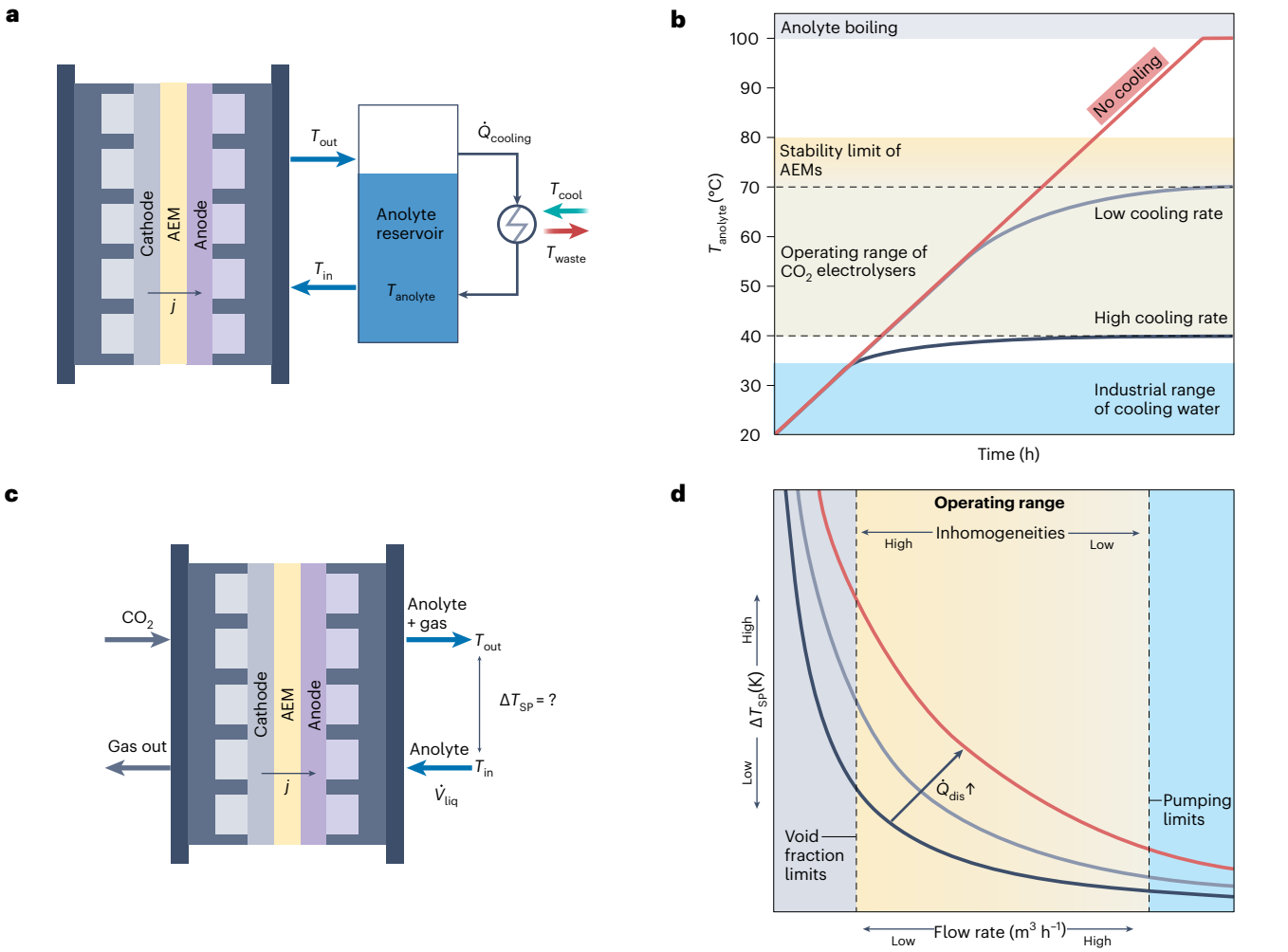

Fig. 2 | Operable temperature range and single-pass spatial temperature gradient. a, Operable temperature for CO_2E stacks operating under a current density (j) with applied cooling at the anolyte circuit using a cooling heat duty $\dot{Q}_{cooling}$, cooling agent temperature T_{cool} and return temperature T_{waste}. **b**, Development of the anolyte temperature $T_{anolyte}$ over operation time. The maximum anolyte temperature is imposed by the AEM stability. The electrolyte temperature at the electrolyser inlet (T_{in}) is equal to $T_{anolyte}$ and is lower than the outlet temperature of the electrolyser (T_{out}). The minimum temperature is given by the temperature level T_{cool} and the applicable cooling rate of the heat exchanger transporting the heat duty. **c**, Analysis of the single-pass spatial temperature gradient ΔT_{SP}, which influences the level of inhomogeneities to the CO_2 stack. **d**, Development of ΔT_{SP} depends on the anolyte flow rate $\dot{V}_{liq}$ as well as the overall dissipating heat transfer rate $\dot{Q}_{dis}$ from the CO_2E stack and is limited by the pumping cost and operable void fraction. The cooling rate can be further enhanced by additional direct cooling.

increases complexity of the stack. It has been demonstrated that water management in CO_2E MEA cells is already highly complex in homogeneous environments, and spatial temperature variations could exacerbate drying out, condensation or flooding events[30–32].

Temperature effects on the performance of CO_2 electrolysers

The cell performance for CO_2E is influenced by a multitude of phenomena that range from the ångström to the millimetre scale. Table 1 presents an overview of the most relevant phenomena and properties for CO_2E in an MEA cell and thus also an industry-scale CO_2E stack, both at ambient temperature and in the proposed temperature range of 40–70 °C.

As an output metric, the applied cell voltage is one of the most important figures of merit, as the majority of the CO_2E stack costs are governed by the electric power input[33]. Literature reports indicate that a higher temperature is kinetically favourable, and the electrolyte and AEM conductivity will be increased, both decreasing the electric power needed at higher temperatures[9,10]. The benefits of temperature on the cell voltage are illustrated in ref. 13.

On the other hand, there is an almost 2.5-fold decrease in CO_2 solubility between 25 and 70 °C (ref. 34), which could challenge the dissolution of gaseous CO_2 and it reaching the entirety of the catalyst layer[35]. Elevated temperatures could then proportionally lower the maximum current density values towards carbon-based products due to an insufficient CO_2 supply. This would manifest as a lower Faradaic efficiency (FE), a parameter that describes the portion of electrons contributing to a certain product. Selectivity and the FE are considered to be similar in CO_2E. As both higher current densities and an FE of >80% towards carbon-based products is desired to ensure economic feasibility[29], it is important that lower solubilities are not inhibiting the performance. Fortunately, existing reports indicate that highly selective and high-rate CO production on silver can proceed at higher temperatures[7]. In addition, any larger electrolyser stack will undoubtedly require at least mildly elevated pressures to offset pressure drops in the gas and liquid channels. The counter effects of pressure on CO_2 solubility are shown in Fig. 3b.

A secondary effect of temperature is its influence on adsorption–desorption and the reaction kinetics, which can impact the product selectivity. This is particularly the case for copper-based catalysts,

https://doi.org/10.1038/s41560-025-01745-5

Table 1 | Non-exhaustive list of CO_2E stack system properties at various temperatures

Property	Temperature (°C)			Ref.
	25	40	70	
Heat sinks				
Heat capacity ($kJ\,mol^{-1}\,K^{-1}$)				
c_{p,H_2O}	4.178	4.179	4.192	22
c_{p,CO_2}	0.849	0.858	0.894	22
Density ($kg\,m^{-3}$)				
ρ_{H_2O}	998.0	991.1	977.5	22
ρ_{CO_2}	1.785	1.587	1.546	22
Salt formation				
Salt solubility ($mol\,l^{-1}$)				
$CsHCO_3$	12.91[a]	16.11[a]	23.93[a]	44
Cs_2CO_3	8.11[a]	8.77[a]	9.59[a]	44
$KHCO_3$	3.63	4.53	6.73	45
K_2CO_3	8.17	8.47	9.66	45
Water management/membrane[b]				
Conductivity ($mS\,cm^{-1}$)				
σ_{OH^-}	72.4	90.8	127.7	46
$\sigma_{HCO_3^-}$	26.3	38.2	60.1	46
Gas loading ($g_{H_2O}\,kg_{CO_2}^{-1}$)				
w_{sat,H_2O,CO_2}	12.29	30.84	193.96	47
CO_2 solubility ($mmol_{CO_2}\,l_{H_2O}^{-1}\,atm^{-1}$)				
k_{CO_2,H_2O}	34.06	23.89	14.90	34
Electrochemical properties[c]				
Thermoneutral potential (V)				
$U_{th,CO_2\rightarrow CO}$	1.467	1.474	1.488	48
$U_{th,CO_2\rightarrow C_2H_4}$	1.219	1.222	1.229	48
$U_{th,H_2O\rightarrow H_2}$	1.481	1.494	1.519	48

Relevant system properties for the system's heat sinks, salt formation, water management/membrane and electrochemical properties. [a]Solubility values for $CsHCO_3$ and Cs_2CO_3 are extrapolated from 15 °C via correlation to the respective $KHCO_3$ and K_2CO_3 temperature trends. [b]Conductivity (σ) values of Sustainion X37 in 1M KOH and 1M $KHCO_3$, respectively. [c]Thermoneutral potential (E_{th}) values of the global reaction assuming the oxygen evolution reaction at the anode.

which see a wider yield of C_1 and C_2 products due to the moderate binding energy of intermediate CO. Whereas limited datasets exist for testing copper at higher temperatures, experiments show that higher temperatures can result in increased selectivity towards carbon-based products versus hydrogen at a current density of 300 mA cm^{-2}. The product distribution, however, shifts away from products such as ethylene and ethanol, leaving CO as the dominant product potentially due to the weakening of CO binding[9]. Thus, the desired optimal temperature is influenced markedly by the temperature-dependent selectivity towards the targeted products while a sufficient supply of CO_2 to the catalyst surface must be maintained.

An upside of higher temperatures is the increased solubility of (bi)carbonate salts, mitigating salt formation[36]. Instead, however, we predict that water management from the anode to the cathode could become a new central challenge for CO_2E. Simulations indicate that H_2O availability at the cathode is a potential bottleneck for the system[37], whereas experiments highlight the C_{2+} selectivity effects of higher and lower water activities[38]. At higher temperatures, the selectivity of membranes usually decreases due to enhanced swelling, implying increased crossover of cations[21,39]. Although the water delivery to the cathode catalyst layer should be easier, the flooding potential increases, combined with the decreasing capillary pressure of the gas diffusion electrode[27]. In addition, the increased saturation level of the CO_2 gas and the higher water vapour pressure increases the danger of drying out if relative humidities are too low[40]. Thus, without proper humidification one could see accelerated salt precipitation, despite the higher solubilities mentioned above. Furthermore, a drier membrane shows a lower conductivity and thus higher overpotentials[19,39].

These brief discussions highlight how sensitive CO_2E is to temperature, and thus how challenging it is to operate under optimal conditions. Depending on the scale of the present internal temperature gradient, spatial dependences can induce even higher complexity. The discussions above indicate that the optimal temperature within the operable temperature range will be application-specific, influenced by a multitude of phenomena and generally as high as possible before voltage advantages are overshadowed by limiting phenomena[41].

Heat recuperation is key for high process efficiencies

We showed that heat must be removed directly from the stack or from the anolyte circuit (see Fig. 2a). Here we briefly show that heat recuperation through secondary processes has the potential to effectively increase the energy efficiency of CO_2 electrolysers. To illustrate this point we can consider three cases that are representative but not exhaustive for scenarios dealing with the dissipated heat. For discussion, we assume that the dissipated heat from the electrolyser system is at 50 °C (see Fig. 4).

The base case 'W' represents the scenario in which the dissipated heat is not used and thus needs to be removed, requiring additional cooling costs. This results in an energy penalty and a process efficiency η_W that is below the energy efficiency of the CO_2E stack.

In a second scenario, labelled case 'A', the 50 °C waste heat is upgraded via a heat pump to 110 °C, giving it higher utility for industrial processes such as downstream separation. An additional power requirement P_A for the heat pump is then needed, but the upgraded temperature results in recovery of the electrolyser system's heat, boosting the process efficiency. The increase in process efficiency η_A depends on the efficiency of the heat pump, which generally decreases with an increase in the temperature gap ΔT_{HP} to be bridges by the heat pump[42]. This case is representative of any process that needs heat input on a substantially higher temperature level than the operation temperature of the stack.

In the third scenario, case 'B', the dissipated heat is valorized directly with little to no upgrading. Here we take the example of district heating in the case where the CO_2E stack is located next to a decentralized heating system. Consequently, the heat pump power requirement P_B, if needed at all, is lower than P_A, meaning that η_B is greater than η_A. For an exact quantification of the efficiency of the processes, the exit temperature levels for cases A and B need to be known. However, the above argumentation shows that a higher operation temperature of the stack generally benefits the heat recuperation. All in all, heat recuperation could increase the energy efficiency of the system substantially, if the CO_2E stack is considered not only as a power sink and a production unit but also as a low-temperature heat source. We note that, in general CO_2E, the heat utility will be low due to the absolute temperature limit of 100 °C. Heat recuperation is then more valuable and essential for alternative technological routes, for example, the reverse water–gas shift reaction or in solid-oxide electrolysers.

Outlook

Literature reports on CO_2E often discuss the need for scale-up and operating under industrially relevant conditions[1,2,43]. In this Perspective we stress that a component of these conditions is operating in the range of 40–70 °C. The field of CO_2E and especially the understanding

https://doi.org/10.1038/s41560-025-01745-5

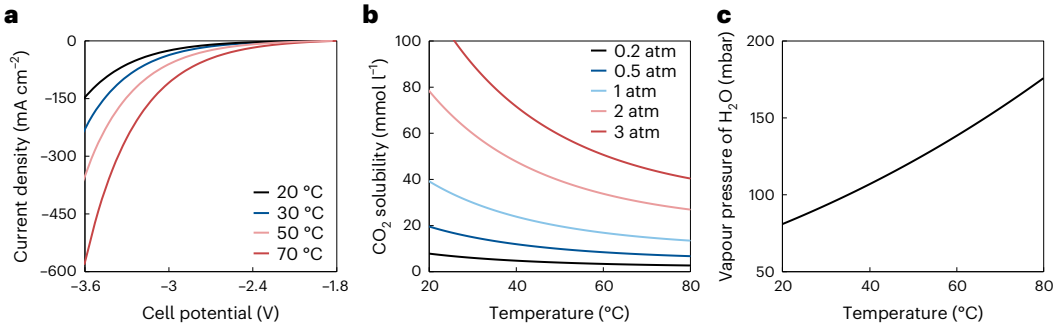

Fig. 3 | Effect of temperature on relevant system properties. a, Impact of temperature on the cell potential–current density curve of an MEA cell, showing faster kinetics with increasing temperature. Data from ref. 9. **b**, Solubility of CO_2 in water as a function of temperature at different partial pressure levels of CO_2, indicating the increased mass transfer resistance regarding CO_2 at elevated temperatures. **c**, Vapour pressure of H_2O as a function of temperature, which indicates the potential danger of dry zones at elevated temperatures. Property data for **b** and **c** from refs. 9,22,34.

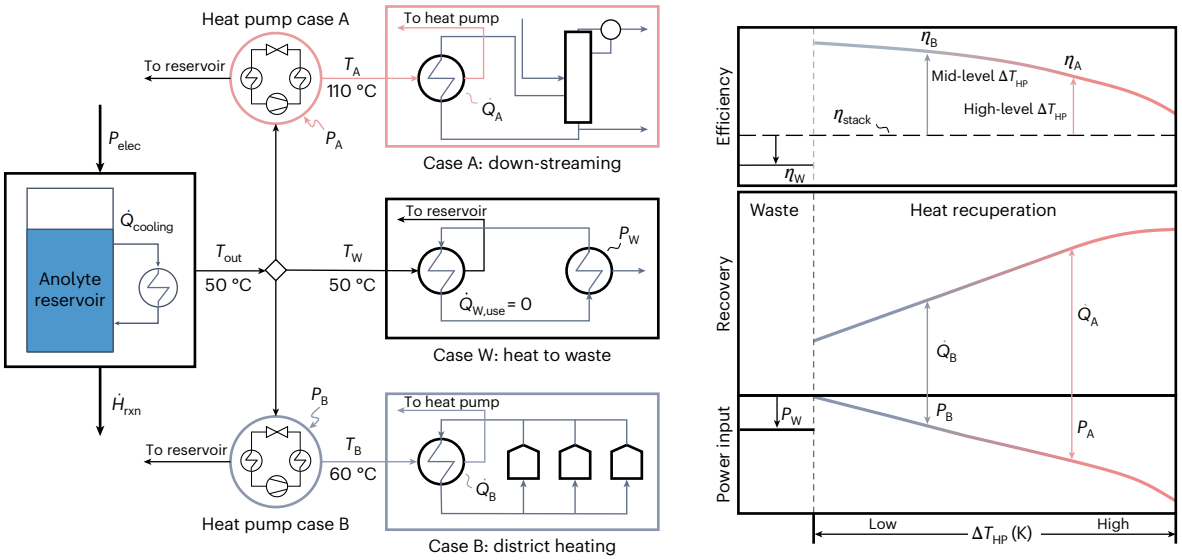

Fig. 4 | Heat recuperation and impact on achievable process efficiencies. Heat that is dissipated from the CO_2E stack, which has a power input P_{elec} that is used partly for the generation of products governed by the reaction enthalpy rate $\dot{H}_{rxn}$ and is countered at the anolyte reservoir by the cooling heat duty $\dot{Q}_{cooling}$, can be reused to enhance the process efficiency. Three use cases are depicted here. Case B represents district heating, as an example of processes that are on a similar temperature level T_B as the heat duty temperature level T_{out}. The efficient heat pumping, due to the low temperature gap (ΔT_{HP}) that is to be bridged, brings a high process efficiency (η_B). Case A represents down-streaming, as an example of processes that are on a substantial higher temperature level T_A compared with T_{out}. The process efficiency η_A decreases in comparison with η_B as the higher heat pumping requirement P_A is not offset by the gain in the reusable heat transfer rate $\dot{Q}_A$ relative to the reusable heat transfer rate $\dot{Q}_B$ and the heat pumping requirement P_B. Case W represents the absence of heat recuperation meaning the reusable heat transfer rate in case W ($\dot{Q}_{W,use}$) equals zero. The power penalty P_W is imposed to meet the energy requirements for cooling down T_W, which is equal to T_{out}, leading to a process efficiency η_W that is below the stack efficiency η_{stack}. Any energy inputs or outputs, except $\dot{Q}_A$ and $\dot{Q}_B$, within the district heating or down-streaming scenarios, are not part of the system balance displayed here.

of relevant phenomena in MEA cells is rapidly expanding, and shifting to testing at elevated temperatures prevents potential unwelcome surprises at the scale-up stage. Furthermore, the means of heat removal from a stack, via either the anolyte or integrated cooling channels, has implications for the design and operation of the electrolyser. Consequently, research areas such as flow field design and durability testing need to have heat management or higher temperature, respectively, in mind. In addition, modelling and in situ analysis, whose outcomes are temperature-dependent, should incorporate these assertions to better characterize a scaled-up CO_2E system[30–32].

A key aspect of the above reasoning is that the accessibility of performing research at 40–70 °C is important but non-trivial. Thousands of researchers are actively working in CO_2E, with a breadth of scientific backgrounds and access to equipment. Engineering systems with controlled and measurable temperature and CO_2 humidities are then a very real barrier to shifting away from research under ambient conditions. Ideally, these controlled set-ups include not only experimental electrolyser test benches but also in situ characterization methods as much as possible. Thus, we encourage the sharing of well-implemented higher-temperature testing set-ups across the community.

In summary, we argue that industry-scale CO_2E stacks will inevitably heat up, causing both predictable and unpredictable effects on efficiency, stability and operation. By incorporating these realities into our methodologies and hypotheses, it is hoped that we can shorten the development time from current laboratory scale to industrial application.

References

1. Barecka, M. H. & Ager, J. W. Towards an accelerated decarbonization of the chemical industry by electrolysis. *Energy Adv.* **2**, 268–279 (2023).

2. Segets, D., Andronescu, C. & Apfel, U.-P. Accelerating CO_2 electrochemical conversion towards industrial implementation. *Nat. Commun.* **14**, 7950 (2023).
3. Burdyny, T. & Mulder, F. M. Scale-up of CO_2 and CO electrolyzers. *Joule* **8**, 2449–2452 (2024).
4. Petrov, K. V. et al. Bipolar membranes for intrinsically stable and scalable CO_2 electrolysis. *Nat. Energy* https://doi.org/10.1038/s41560-024-01574-y (2024).
5. Ozden, A. et al. Energy- and carbon-efficient CO_2/CO electrolysis to multicarbon products via asymmetric ion migration–adsorption. *Nat. Energy* **8**, 179–190 (2023).
6. Reichbauer, T. et al. Electrical energy input efficiency limitations in CO_2-to-CO electrolysis and attempts for improvement. *Electrochem. Sci. Adv.* **4**, e2300024 (2024).
7. Endrődi, B. et al. High carbonate ion conductance of a robust PiperION membrane allows industrial current density and conversion in a zero-gap carbon dioxide electrolyzer cell. *Energy Environ. Sci.* **13**, 4098–4105 (2020).
8. Technical targets for proton exchange membrane electrolysis. *US Department of Energy* (accessed 20 March 2025); https://www.energy.gov/eere/fuelcells/technical-targets-proton-exchange-membrane-electrolysis
9. Giron Rodriguez, C. A. et al. Insights into zero-gap CO_2 electrolysis at elevated temperatures. *EES Catal.* **2**, 850–861 (2024).
10. Vos, R. E. et al. How temperature affects the selectivity of the electrochemical CO_2 reduction on copper. *ACS Catal.* **13**, 8080–8091 (2023).
11. Schellekens, M. P., Raaijman, S. J., Koper, M. T. M. & Corbett, P. J. Temperature-dependent selectivity for CO electroreduction on copper-based gas-diffusion electrodes at high current densities. *Chem. Eng. J.* **483**, 149105 (2024).
12. Krause, R. et al. Industrial application aspects of the electrochemical reduction of CO_2 to CO in aqueous electrolyte. *Chem. Ing. Tech.* **92**, 53–61 (2020).
13. Quentmeier, M., Schmid, B., Tempel, H. & Eichel, R.-A. Modular CO_2-to-CO electrolysis short-stack design—impact of temperature gradients and insights into position-dependent cell behavior. *ACS Sustain. Chem. Eng.* **12**, 3876–3885 (2024).
14. Crandall, B. S. et al. Kilowatt-scale tandem CO_2 electrolysis for enhanced acetate and ethylene production. *Nat. Chem. Eng.* **1**, 421–429 (2024).
15. Wakerley, D. et al. Gas diffusion electrodes, reactor designs and key metrics of low-temperature CO_2 electrolysers. *Nat. Energy* **7**, 130–143 (2022).
16. Lees, E. W., Mowbray, B. A. W., Parlane, F. G. L. & Berlinguette, C. P. Gas diffusion electrodes and membranes for CO_2 reduction electrolysers. *Nat. Rev. Mater.* **7**, 55–64 (2022).
17. Iglesias van Montfort, H.-P. et al. An advanced guide to assembly and operation of CO_2 electrolyzers. *ACS Energy Lett.* **8**, 4156–4161 (2023).
18. Kibria, M. G. et al. Electrochemical CO_2 reduction into chemical feedstocks: from mechanistic electrocatalysis models to system design. *Adv. Mater.* **31**, 1807166 (2019).
19. Weng, L.-C., Bell, A. T. & Weber, A. Z. Towards membrane-electrode assembly systems for CO_2 reduction: a modeling study. *Energy Environ. Sci.* **12**, 1950–1968 (2019).
20. Hansen, K. U., Cherniack, L. H. & Jiao, F. Voltage loss diagnosis in CO_2 electrolyzers using five-electrode technique. *ACS Energy Lett.* **7**, 4504–4511 (2022).
21. Garg, S., Giron Rodriguez, C. A., Rufford, T. E., Varcoe, J. R. & Seger, B. How membrane characteristics influence the performance of CO_2 and CO electrolysis. *Energy Environ. Sci.* **15**, 4440–4469 (2022).
22. Incropera, F. P., DeWitt, D. P., Bergman, T. L. & Lavine, A. S. *Fundamentals of Heat and Mass Transfer* 6th edn (Wiley, 2007).
23. Wijaya, G. H. A., Im, K. S. & Nam, S. Y. Advancements in commercial anion exchange membranes: a review of membrane properties in water electrolysis applications. *Desalin. Water Treat.* **320**, 100605 (2024).
24. *Industrial Cooling Systems* (Callens, accessed 19 September 2024); https://www.callens.eu/en/air-technology/industrial-cooling
25. Mokhatab, S., Poe, W. A. & Mak, J. Y. in *Handbook of Natural Gas Transmission and Processing: Principles and Practices* 537–578 (Elsevier, 2019); https://doi.org/10.1016/B978-0-12-815817-3.00018-6
26. Toghyani, S., Afshari, E., Baniasadi, E. & Atyabi, S. A. Thermal and electrochemical analysis of different flow field patterns in a PEM electrolyzer. *Electrochim. Acta* **267**, 234–245 (2018).
27. Rossen, A., Daems, N., Choukroun, D. & Breugelmans, T. Differential pressure across a gas diffusion electrode controls efficiency of liquid-fed electrolyzers for CO_2 electroreduction at elevated temperatures. *ACS Sustain. Chem. Eng.* https://doi.org/10.1021/acssuschemeng.4c01908 (2024).
28. Deng, X., Yang, F., Li, Y., Dang, J. & Ouyang, M. Quantitative study on gas evolution effects under large current density in zero-gap alkaline water electrolyzers. *J. Power Sources* **555**, 232378 (2023).
29. Belsa, B. et al. Materials challenges on the path to gigatonne CO_2 electrolysis. *Nat. Rev. Mater.* https://doi.org/10.1038/s41578-024-00696-9 (2024).
30. Moss, A. B. et al. In operando investigations of oscillatory water and carbonate effects in MEA-based CO_2 electrolysis devices. *Joule* **7**, 350–365 (2023).
31. Disch, J. et al. High-resolution neutron imaging of salt precipitation and water transport in zero-gap CO_2 electrolysis. *Nat. Commun.* **13**, 6099 (2022).
32. Joensen, B. Ó. et al. Unveiling transport mechanisms of cesium and water in operando zero-gap CO_2 electrolyzers. *Joule* https://doi.org/10.1016/j.joule.2024.02.027 (2024).
33. Sisler, J. et al. Ethylene electrosynthesis: a comparative techno-economic analysis of alkaline vs membrane electrode assembly vs CO_2–CO–C_2H_4 tandems. *ACS Energy Lett.* **6**, 997–1002 (2021).
34. García De Arquer, F. P. CO_2 electrolysis to multicarbon products at activities greater than 1 A cm^{-2}. *Science* **367**, 661–666 (2020).
35. Nesbitt, N. T. et al. Liquid–solid boundaries dominate activity of CO_2 reduction on gas-diffusion electrodes. *ACS Catal.* **10**, 14093–14106 (2020).
36. Biemolt, J., Singh, J., Prats Vergel, G., Pelzer, H. M. & Burdyny, T. Preventing salt formation in zero-gap CO_2 electrolyzers by quantifying cation accumulation. *ACS Energy Lett.* **10**, 807–814 (2025).
37. Nesbitt, N. T. & Smith, W. A. Water and solute activities regulate CO_2 reduction in gas-diffusion electrodes. *J. Phys. Chem. C* **125**, 13085–13095 (2021).
38. Zhang, H., Gao, J., Raciti, D. & Hall, A. S. Promoting Cu-catalysed CO_2 electroreduction to multicarbon products by tuning the activity of H_2O. *Nat. Catal.* **6**, 807–817 (2023).
39. Luo, X., Rojas-Carbonell, S., Yan, Y. & Kusoglu, A. Structure–transport relationships of poly(aryl piperidinium) anion-exchange membranes: effect of anions and hydration. *J. Membr. Sci.* **598**, 117680 (2020).
40. Wheeler, D. G. et al. Quantification of water transport in a CO_2 electrolyzer. *Energy Environ. Sci.* **13**, 5126–5134 (2020).
41. Hurkmans, J.-W., Pelzer, H. M., Burdyny, T., Peeters, J. & Vermaas, D. A. Heating dictates the scalability of CO_2 electrolyzer types. *EES Catal.* https://doi.org/10.1039/D4EY00190G (2025)
42. Jensen, J. K. et al. Heat pump COP, part 2: generalized COP estimation of heat pump processes. In *Proc. 13th IIR Gustav Lorentzen Conference on Natural Refrigerants (GL2018)* (International Institute of Refrigeration, 2018); https://doi.org/10.18462/IIR.GL.2018.1386

43. Siegmund, D. et al. Crossing the valley of death: from fundamental to applied research in electrolysis. *JACS Au* **1**, 527–535 (2021).
44. Garg, S. et al. How alkali cations affect salt precipitation and CO_2 electrolysis performance in membrane electrode assembly electrolyzers. *Energy Environ. Sci.* **16**, 1631–1643 (2023).
45. *Solubility Table for Water at Temperature* (Merck, accessed 10 September 2024); https://www.sigmaaldrich.com/NL/en/support/calculators-and-apps/solubility-table-compounds-water-temperature
46. *Sustainion® Anion Exchange Membranes* (Dioxide Materials, accessed 11 September 2024); https://dioxidematerials.com/technology/sustainion-membranes/
47. Vaughan, G. L. & Carrington, C. G. Psychrometric properties of a moist carbon dioxide atmosphere. *Int. J. Food Prop.* **1**, 77–87 (1998).
48. Zheng, Y. et al. Energy related CO_2 conversion and utilization: advanced materials/nanomaterials, reaction mechanisms and technologies. *Nano Energy* **40**, 512–539 (2017).

Acknowledgements

This project received funding from project "e-Heat: Understanding and controlling heat to enable large scale electrolysers" (NWO OTP 19757).

Author contributions

Conceptualization was by H.M.P., D.V. and T.B. Visualization was by H.M.P., N.K., D.V. and T.B. The original draught was written by H.M.P., N.K., D.V. and T.B., and the manuscript was reviewed and edited by H.M.P., D.V. and T.B. Funding acquisition was by D.V. and T.B.

Competing interests

The authors declare no competing interests.

Additional information

Correspondence should be addressed to Henri M. Pelzer or Thomas Burdyny.

Peer review information *Nature Energy* thanks Feng Jiao, Guenter Schmid and the other, anonymous, reviewer(s) for their contribution to the peer review of this work.